Inadequacy of current approaches for characterizing membrane transport properties at high salinities

Yuanzhe Liang [a], Alexander V. Dudchenko [b], Meagan S. Mauter [a,*]

[a] *Department of Civil & Environmental Engineering, Stanford University, Stanford, CA, 94305, USA*
[b] *Applied Energy Division, SLAC National Accelerator Laboratory, Menlo Park, CA, 94025, USA*

A B S T R A C T

Cost optimal design of osmotic membrane processes requires an accurate estimate of membrane transport parameters across their full operational range. However, standard approaches for estimating these parameters rely on empirical methods, the accuracy of which remains unquantified as a function of temperature, salinity, and measurement error. Herein, we present a systematic accuracy analysis of previously developed methods for estimation of membrane transport properties in reverse osmosis, high-pressure reverse osmosis, forward osmosis, pressure retarded reverse osmosis, and osmotically assisted reverse osmosis. We use a Monte Carlo approach to sample the full range of feasible membrane water permeabilities, salt permeabilities, structural parameters, and operating conditions for these processes. These material and process parameters are then incorporated into a physical transport model for each process. Our analysis shows that the statistical uncertainty of current empirical methods for estimating membrane parameters increases by 5 times from low-salinity to high-salinity conditions. The result of this work demonstrates that empirical methods are inadequate for precisely estimating membrane transport properties at high salinity and highlight a critical need for the development of statistically validated higher accuracy methods.

1. Introduction

The design of optimal membrane-based desalination systems requires accurate estimates of membrane performance across the full range of operational salinities and temperatures [1–3]. Extending this operational range for enhanced recovery and separation efficiency is a design feature of several emerging processes, including osmotically assisted reverse osmosis (OARO) [1], cascading osmotically mediated reverse osmosis (COMRO) [4], low-salt-rejection reverse osmosis (LSSRO) [5], high pressure reverse osmosis (HPRO) [6], closed circuit reverse osmosis (CCRO) [7], batch reverse osmosis [8], and forward osmosis (FO) [9]. These processes are often designed as multi-stage systems, further widening the range of temperature and salinity that membranes experience [9]. Accurately estimating the water permeability (A), salt permeability (B), and structural parameter (S) of these membranes across the range of operating conditions is critical to cost optimal process design.

While membrane parameters are commonly treated as constants in process design, transport theory suggests that water and salt permeability are a function of solution salinity and temperature. Free volume theory states that the transport of water and salt in membrane materials increases with an increase in fractional water volume or water uptake by the polymer [10,11]. This theory is supported by experimental work using positron annihilation lifetime spectroscopy (PALS) which quantitatively correlated increase in free volume with increase in polymeric membrane water and salt permeability [12–14].

Theory also suggests that increased external salt concentration or decreased temperature decreases the thermodynamic activity of water in the solution and induces osmotic de-swelling of the polymeric membrane. The reduced water uptake leads to a decrease in water and salt permeability of the membrane [12,15–19]. For charged membrane materials, such as polyamide (PA), Donnan theory states that salt transport increases with decreases in polymer charge and increases in salinity, which screens the polymer charge [19–24].

Experimental observations also suggest the transport of water and salt in polymers is dependent on salinity and temperature. The effect of salinity on transport of water and salt in polymers varies between uncharged and charged polymers [10]. For instance, Jang et al. reported that the water uptake in uncharged poly (ethylene glycol diacrylate) polymers decreased by 20% when the external NaCl concentration

* Corresponding author.
  E-mail address: mauter@stanford.edu (M.S. Mauter).

increased from 0 mol/L to 1 mol/L, resulting in a 15% decrease in salt permeability [25]. In contrast, Geise et al. reported that the salt permeability of charged sulfonated polymers increased by 10 times when the polymer water content decreased by 50% when NaCl concentration increased from 0 mol/L to 1 mol/L [26]. Past work has also extensively documented the increase in permeation of water and salt permeability with the increase in temperature in reverse osmosis (RO) and FO experiments. For instance, Ng et al. observed a ~30% increase in water permeance in FO experiment when the ambient temperature rose from 30 °C to 50 °C [27]. Similarly, Goosen et al. reported a ~50% increase in water permeance in RO experiment when the feed temperature increased from 20 °C to 40 °C [28].

Despite theoretical and experimental evidence that water and salt transport parameters are a function of feed water salinity and temperature, efforts to rigorously quantify these effects over the operational range of emerging processes are incomplete. While relating membrane performance to ex-situ structure is standard practice [12,29], we are unaware of direct methods for in-situ/operando measurement of membrane transport properties. Instead, researchers use indirect

measurements coupled with empirical methods for approximating membrane parameters. The accuracy of these estimates is dependent on the completeness of the empirical model, the validity of the model across a wide range of salinities and temperatures, and the robustness of the empirical method to measurement error. As a result, we have limited ability to resolve changes in membrane transport parameters introduced by changes in salinity, pressure, or temperature. This resolution is particularly limited at high salinities, as evidenced by the inconclusive determination of trends in B values with increase in salinity in several recent studies [4,30].

Current empirical approaches for estimating membrane parameters across a wide range of salinities and temperatures suffer several shortcomings. When pressure is the sole driving force of the process (i.e., RO, CCRO, and batch RO), water permeability (A) and salt permeability (B) are calculated by fitting spatially and temporally averaged experimental operating conditions (e.g., pressure, flow rate) and measured water flux and salt flux to a classic RO mass transport model (Fig. 1A) [31]. This RO model assumes that external concentration polarization is either well defined by the mass transport model or is negligible due to the inclusion
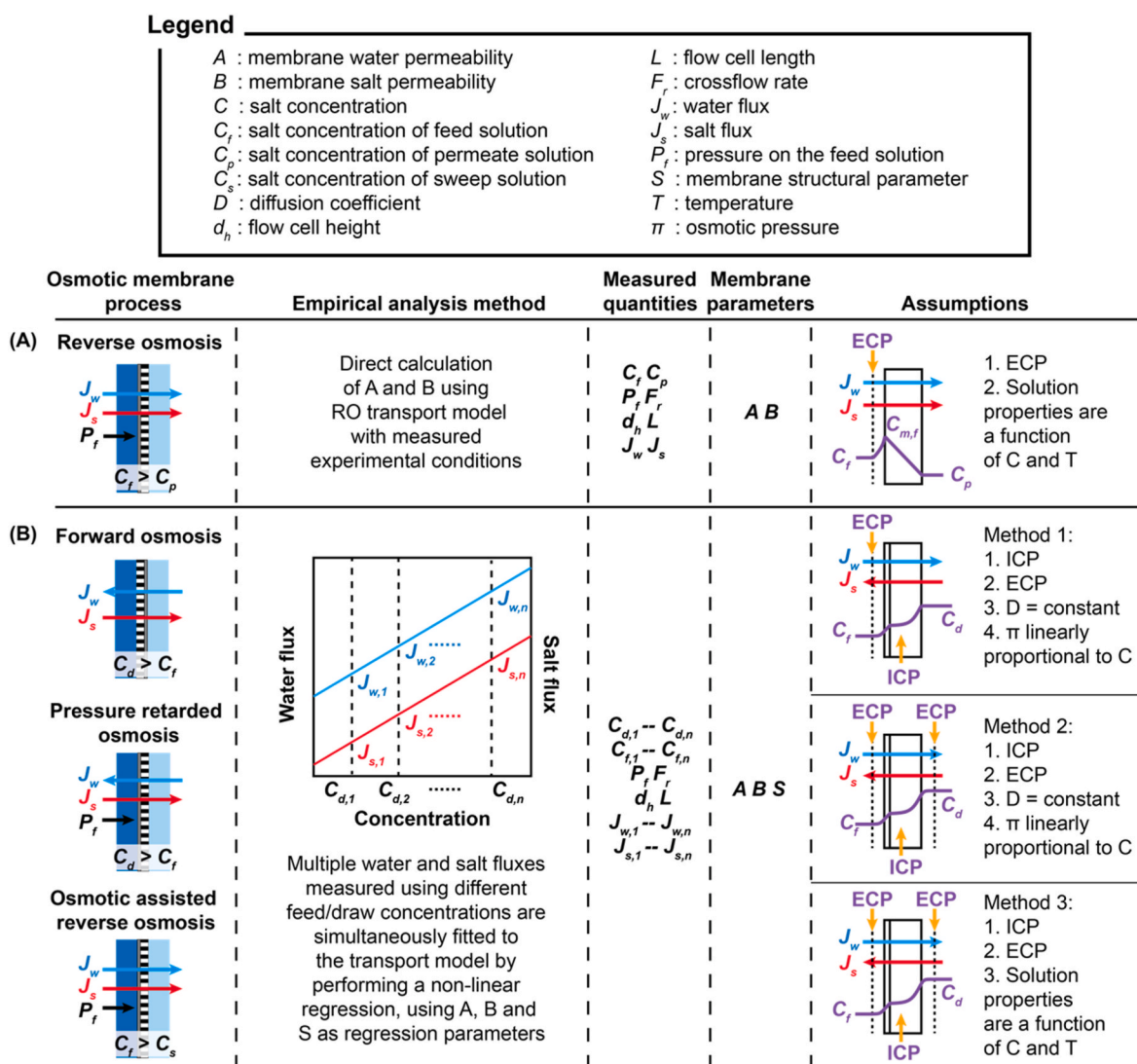

Fig. 1. Empirical methods used for estimation of membrane water, salt permeability, and structural parameters in (A) reverse osmosis (RO), (B) forward osmosis (FO), pressure retarded reverse osmosis (PRO), and osmotic assisted reverse osmosis (OARO). In RO and HPRO, water and salt permeability coefficients are directly calculated using the RO transport model with measured experimental conditions. In FO, PRO, and OARO, a single experiment is divided into multiple stages, each using a different concentration of draw/feed solution. The measured water and salt flux in each stage are simultaneously fitted to the respective transport model by performing a non-linear regression, using A, B, and S as regression parameters. Method 1 is developed by Tiraferri et al. for FO [33], method 2 is developed by Nagy et al. and Bui et al. for FO [34,35], method 3 is developed by Chowdhury et al. and Martin et al. for FO and PRO [36,37].

of a spacer. Rigorous implementations of this approach also account for the effect of solute concentration and temperature on solution properties. Despite the well established approach for calculating A and B parameters using the classical RO model, the accuracy of this direct calculation method is contingent upon the precise measurement of process parameters. Its application is further limited to feed salinities of less than ~100 g/L as standard RO systems and membranes are designed to operate below ~85 bar. Only recently has work explored significantly higher pressures [6,32]. In addition, the spatial and temporal averaged values obtained from this approach are only valid if the inlet and outlet feed salinities and temperatures are approximately equal.

Existing methods for measuring A and B parameters in osmotically driven membrane processes rely on assumptions that further hinder accurate estimates of membrane parameters across a wide range of salinities and temperatures. In contrast to RO process, osmotic processes need to account for mass transfer resistance in the asymmetric membrane support layer, which is captured by the structural parameter (S). Reported approaches for FO, pressure retarded reverse osmosis (PRO), and OARO require simultaneous estimation of three membrane parameters. This is achieved by collecting water and salt flux data over several different draw/feed solution concentrations [33] and using non-linear regression, with A, B, and S as regression parameters, to simultaneously fit the measured water and salt fluxes for each condition to the respective transport model (Fig. 1B) [33]. Unfortunately, these methods assume membrane parameters are not a function of salinity, thus introducing theoretical inconsistency into the parameter estimates and introducing uncertainty into whether these methods can be applied to characterize how A and B vary with salinity.

Reporting of membrane parameters is further complicated by the breadth of available empirical methods, the accuracy of which is dependent on their underlying assumptions. For example, one of the most common methods for estimating FO membrane parameters developed by Tiraferri et al. assumes a linear relationship between osmotic pressure and salinity, a constant diffusion coefficient, and negligible mass transfer in the feed-membrane boundary layer because DI water was used. These assumptions produce inaccurate estimates of membrane parameters when this method is applied in concentrated solutions [33]. Nagy et al. and Bui et al. proposed a revised method that includes both ECPs in the feed- and draw-boundary layers. While this modification enhances the validity of the model in non-dilute draw solutions [34,35], the method omits any dependence of solution properties on salinity and temperature. Chowdhury et al. and Martin et al. address this shortcoming by introducing a model that explicitly captures thermophysical solution properties as a function of temperature and concentration [36,37].

In addition to the errors introduced by simplifying assumptions, uncertainty in experimental measurements can introduce large errors in empirical methods. Tiraferri et al. reported the average errors of estimated A, B, and S increased to 14% when the errors in flux measurements increased to 15% in FO experiments [33]. Our prior work demonstrated that errors in measured solution properties and process conditions in membrane distillation induced a high degree of uncertainty in estimates of membrane permeability and heat transfer rate [38]. Explicitly understanding the relationship between measurement uncertainty and error of estimated membrane parameters is critical for designing experiments that maximize empirical method accuracy.

In this work, we evaluate the accuracy of the methods for estimating membrane parameters in RO/HPRO, FO, PRO, and OARO. We simulate membrane processes using standard mass balance models for RO, FO, PRO, and OARO. We then compare the effects of methodological and experimental error under assumptions of constant A and B to those for concentration-dependent A and B parameters generated using Flory-Rehner theory, free-volume theory, and Donnan theory. In both cases, we assume S is independent of concentration. The sampling ranges of A, B, and S parameters are representative of typical and state-of-the-art cellulose acetate (CTA) and thin-film-composite polyamide (TFC-PA)

membranes reported in the literature. In each analysis, we generated 10,000 datasets of water and salt flux for RO/HPRO, 40,000 datasets of water and salt flux for FO, PRO, and OARO. The accuracy and robustness of the empirical methods are assessed by analyzing each simulation with no error and with varying levels of random errors in measured parameters. Finally, we evaluate the accuracy of empirical methods in estimating A, B, and S in the four osmotic processes with constant and concentration-dependent A and B as a function of method completeness, feed salinity, and measurement error.

2. Methods

2.1. Generation of membrane parameter data

We generated a set of constant membrane parameters and concentration-dependent membrane parameters. The range of constant A and B parameters is defined by values reported in the literature (Table 1) [2,33] and a Monte-Carlo (MC) approach is used to randomly sample this range. The concentration-dependent A and B values are generated using Flory-Rehner, free-volume, and Donnan theory [25, 39–42] (Supplementary Section A). In brief, we use an MC approach to sample material properties that include pre-polymerization polymer volume, φ_1, polymer volume fractions in the swollen state, $\varphi_{2,w}$, cross-linking degree, ν_e, fixed charge concentration, C_A^m, active layer thickness, h, volume fractions of hydrophilic polymers, φ, the fraction of material that behaves as an ideal Donnan ion exchange material, f_D, and process

Table 1
Parameter ranges used for data set generation.

Input parameter (unit)	Minimum value	Maximum value
Membrane properties		
Pre-polymerization polymer volume, φ_1	0.9	1
Polymer volume fractions in the swollen state, φ_{2w}	0.75	0.9
Crosslinking degree, ν_e (mmol.cm^{-3})	1	5
Fraction of the material that behaves as an ideal Donnan ion exchange material, f_D	0	1
Fixed charge concentration, C_A^m (eq.L^{-1})	0	0.5
Active layer thickness, h (um)	0.1	2
Volume fractions of hydrophilic polymer, $\varnothing^{hydrophilic}$	0.8	1
Membrane parameter		
Water permeability coefficient, A (L. m^{-2}.h^{-1}.bar^{-1})	0.1	10
Salt permeability coefficient, B (L.m^{-2}. h^{-1})	0.05	1
Structural parameter, S (μm)	200	5000
Module design		
Channel height (cm)	1	10
Length (m)	0.05	0.2
Operation condition		
Feed inflow rate (L.h^{-1})	30	80
Draw inflow rate (L.h^{-1})	30	80
Temperature (°C)	10	50
OARO Feed concentration (g.L^{-1})	5	300
Sweep concentration (g. L^{-1})	1	250
Feed pressure (bar)	1	65
PRO Feed concentration (g.L^{-1})	5	250
Draw concentration (g. L^{-1})	10	300
Feed pressure (bar)	1	65
FO Feed concentration (g.L^{-1})	5	250
Draw concentration (g. L^{-1})	10	300
RO/ Feed concentration (g.L^{-1})	1	200
HPRO Feed pressure (bar)	Feed Osmotic pressure	300
	1.3 * Osmotic pressure of feed concentration	

conditions including feed concentration and temperature. We then use Flory-Rehner theory to estimate water uptake by the polymer for a specific operating condition [25,39–42] (Supplementary Section A). Water uptake is then used to estimate the water and salt sorption coefficients and diffusion coefficients based on the free volume theory and Donnan theory [25,42–45] (Supplementary Section A). Finally, we use these coefficients and the solution-diffusion model to calculate hydraulic water permeability (A) and salt permeability (B) for the specific experimental condition [46,47] (Supplementary Section A). For all cases, we sample the S parameter from values normally reported in the literature using the MC approach.

2.2. Generation of process data

The experimental data for RO/HPRO, FO, PRO, and OARO was simulated using the physical mass transport model of each process that is described in detail in prior literature and in brief in Supplementary Section B. We simulated the full range of operating conditions via random selection of input values from a uniform distribution using the MC approach (Table 1) [48]. The model input parameters consisted of membrane parameters, module design parameters, and operating conditions, while the output data included water flux and salt flux (Fig. 2). We generated two sets of RO data with different methods for sampling applied hydraulic pressure/over pressure (i.e., the pressure over the osmotic pressure of feed solution). In the first RO dataset, we randomly select over pressure in a range from the estimated osmotic pressure of feed solution to 300 bar using a MC approach. In the second RO dataset, we use a fixed over pressure that is equal to 1.3 times of osmotic pressure of feed solution. We choose a ratio of 1.3 to ensure the maximum applied pressure at 200 g/L is close to 300 bar. In both RO/HPRO simulations, we only solve the processes where the rejection rate is equal to or larger than 99%. We generated a total of 10,000 data sets for RO/HPRO and 40,000 data sets for FO, PRO, and OARO. Our selected solver was able to solve ~90% of randomly generated combinations of input data, terminating once the change in water and salt flux was <0.1%. The CDFs of the distribution of values are reported in Supplementary Section C (Supplementary Figs. S1–S4).

2.3. Error addition to data sets

We first evaluate the accuracy of each empirical method without error addition. Next, we evaluate the effect of measurement errors on the accuracy of empirical estimation methods for RO/HPRO, FO, PRO, and OARO processes by adding small or large random errors to a selected set of process parameters and simulated flux data (Fig. 2). We use ±1% for small errors and ±5% for large errors in concentration, flux, flowrate, pressure, Sherwood number, and ±0.5 °C for small errors and ±2.5 °C for large errors in temperature. All errors are randomly generated from a uniform distribution and are added to the inputs prior to analysis by the methods described above. Each data set is analyzed ten times with different errors, expanding the testing data set size from 10,000 to 100,000 for RO/HPRO and from 40,000 to 400,000 for the other processes.

2.4. Parameter estimation method for RO/HPRO

We use a standard method to estimate the membrane water and salt permeability in RO [49] (Fig. 1A). The concentration at the feed side of the membrane is first calculated using Eqn. (1) to account for the effect of external concentration polarization (ECP) in the feed-membrane boundary layer. Then the membrane water permeability (A) and salt permeability (B) are directly calculated using Eqns. (2) and (3):

$$C_{m,f} = C_{b,f} \exp\left(\frac{J_w}{k_f}\right) - \frac{J_s}{J_w}\left[\exp\left(\frac{J_w}{k_f}\right) - 1\right] \tag{1}$$

$$A = \frac{J_w}{\left[(P_f) - (\pi_{m,f}(C_{m,f}) - \pi_p(C_p))\right]} \tag{2}$$

$$B = \frac{J_s}{(C_{m,f} - C_p)} \tag{3}$$

Here, J_w is the experimentally measured water flux, J_s is the experimentally measured salt flux, $C_{b,f}$ is the bulk feed salt concentration, k_f is the mass transfer coefficient, P_f is the hydraulic feed pressure, $\pi_{m,f}$ is the osmotic pressure at the feed-membrane interface, $\pi_{m,p}$ is osmotic pressure in the permeate, and C_p is the salt concentration in permeate.

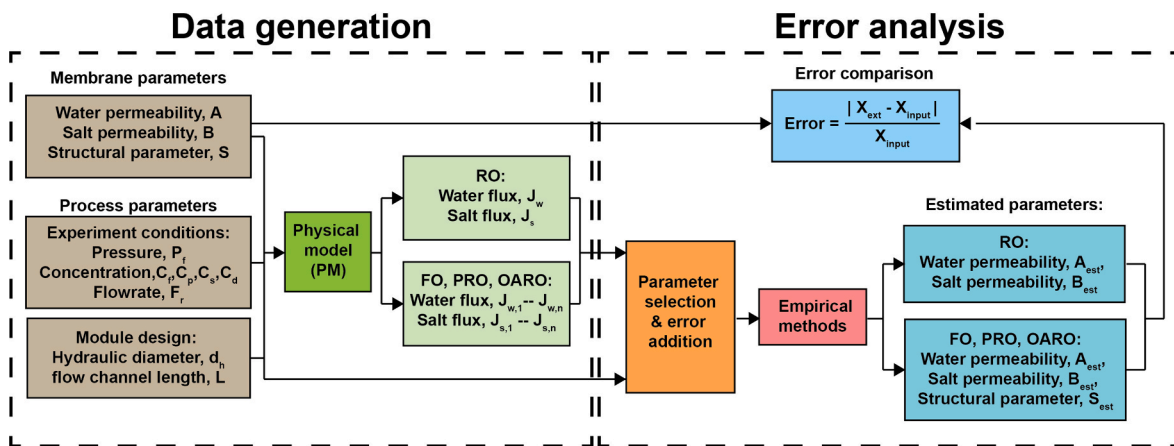Another widely used method for experimentally characterizing RO

Fig. 2. Proposed framework for data simulation and error analysis. The process data for RO, HPRO, FO, PRO, and OARO is simulated using the physical mass transport model (i.e., solution-diffusion model) of each process that balances the mass transfer across the membrane. Two sets of process data are generated, one with constant membrane parameters and the other with concentration-dependent membrane parameters. In the first dataset, the inputs into the model are sampled using a Monte Carlo approach, where membrane parameters and process parameters are varied across a bounded range shown in Table 1. In the second dataset, the concentration-dependent membrane parameters are first generated using Flory-Rehner, free-volume, and Donnan theory from membrane properties and operating conditions that are sampled using a Monte Carlo approach. The calculated membrane parameters and process parameters are then used as inputs into the physical model to simulate the process data. The simulated results and the original process parameters with no error and with varying levels of random errors added in one or more inputs are used to estimate membrane parameters using empirical methods. The accuracy of each empirical method is assessed by comparing the difference between the predicted membrane parameters and the original membrane parameter inputs.

membrane parameters assumes A is pure water permeability, which is constant across the salinity range. The membrane is first tested using DI water as feed, and water permeability is determined by dividing the water flux (J_w) by the applied pressure (ΔP) (Eqn. (4)). The membrane is then tested using a saline feed, and salt permeability is calculated from the rejection rate (R = 1- C_p/C_f), water flux, and mass transfer coefficient (k_f), as shown in Eqn. (5):

$$A = \frac{J_w}{\Delta P} \tag{4}$$

$$B = J_w \frac{1-R}{R} \exp\left(\frac{J_w}{k_f}\right) \tag{5}$$

Despite its broad usage to determine A and B of RO membranes in lab-scale RO experiment, this method does not enable the characterization of A parameters as a function of salinity. Therefore, we will not include this method in this analysis.

2.5. Parameter estimation method for FO, PRO, and OARO

We perform error analysis on three previously reported empirical methods for estimating membrane parameters in FO or PRO (Fig. 1B). These methods also apply to the OARO process. Details of these methods are described in Supplementary Section D (Supplementary Fig. S5). We use a standard differential evolution solver in Scipy to fit a group of four experimental conditions to each empirical method, using A, B, and S as regression parameters [50]. The solver minimizes the normalized difference between estimated and measured fluxes as shown in Eqn. (6) and originally proposed by Tiraferri et al. [33]:

$$E = E_w + E_s = \sum_{i=1}^{n}\left(\frac{J_{w,i}^{est} - J_{w,i}^{input}}{\overline{J_{w,i}^{input}}}\right)^2 + \sum_{i=1}^{n}\left(\frac{J_{s,i}^{est} - J_{s,i}^{input}}{\overline{J_{s,i}^{input}}}\right)^2 \tag{6}$$

Where n is the number of stages and equal to 4 in this study, $\overline{J_{w,i}^{input}}$ is the mean water flux of the four input water fluxes and $\overline{J_{s,i}^{input}}$ is the mean salt flux of the four input salt fluxes. The error at each stage was scaled by the mean input so that each term in Eqn. (6) is weighted equally.

The goodness of the fit was checked using the coefficient of determination as shown in Eqn. (7) and absolute error between the estimated water/salt flux and corresponding input water/salt flux as shown in Eqn. (8) [33]. Our selected solver was able to solve ~85% of randomly generated combinations of input data where the coefficient of determination is larger than 0.95 and the absolute error in water/salt flux is less than 0.1%. The rejection of false solutions leads to a non-uniform distribution of some of the input parameters and output values. The CDFs of the distributions of values are shown in Supplementary Figs. S1–S4.

$$R_w^2 = 1 - \frac{S_{err,w}}{S_{TOT,w}} = 1 - \frac{\sum_{i=1}^{n}\left(J_{w,i}^{est} - J_{w,i}^{input}\right)^2}{\sum_{i=1}^{n}\left(J_{w,i}^{input} - \overline{J_{w,i}^{input}}\right)^2} \tag{7}$$

$$Err_{abs,w,i} = \left|\frac{J_{w,i}^{est} - J_{w,i}^{input}}{J_{w,i}^{input}}\right| \times 100\% \tag{8}$$

2.6. Analysis of empirical method accuracy

We analyze the accuracy of the empirical estimation methods used in RO/HPRO, FO, PRO, and OARO by comparing the estimated membrane parameters solved by each method with those used in the physical models to generate operational data (Fig. 2). In the case of constant membrane parameters, the error is calculated as the difference between the estimated values and original input as shown in Eqn. (9).

$$Err_{abs,X} = \frac{\left|X^{est} - X^{input}\right|}{X^{input}} \times 100\% \tag{9}$$

Here, X^{est} is the estimated membrane parameter (i.e., A, B and S). In the case of concentration-dependent membrane parameters, the error calculation for the RO/HPRO method is also using Eqn. (9). For the method of FO, PRO, and OARO, the error is calculated as the difference between the estimates and the mean of the four input membrane water permeabilities and salt permeabilities (each is corresponding to one of four stages of experimental measurements) as shown in Eqn. (10).

$$Err_{abs,X} = \frac{\left|X^{est} - \overline{X^{input}}\right|}{\overline{X^{input}}} \times 100\% \tag{10}$$

Here, X^{input} is the input membrane parameter (i.e., A and B), and $\overline{X^{input}}$ is the mean of the four values of the input membrane parameters across the simulated experimental conditions.

We group the data in the concentration range from 0 to 50 g/L as the low concentration range for all processes, 150–200 g/L as the high concentration range for HPRO, and 250–300 g/L as the high concentration range for FO, PRO, and OARO. We report the median error and 95th percentile error of estimated membrane parameters as a function of the osmotic process, method sophistication, concentration range, and the error level in input parameters. The median error represents the middle value of the errors in all estimated membrane parameters, and the 95th percentile error represents the value that marks the statistical point where 95% of the errors in estimates are below it. (Supplementary Fig. S6).

3. Results and discussion

Most work assumes that the water and salt permeability of membrane materials remains constant across the operational salinity range of a membrane process. While this simplifying assumption introduces minimal error in steady state RO systems treating brackish or seawater feed streams, theory suggests the potential for large deviations in A and B values when membranes are deployed to concentrate brines to high salinities. Accurately estimating the water permeability and salt permeability of membranes across a broad range of concentrations is thus critical for optimizing the design and operation of emerging high salinity and non-steady state desalination processes.

We begin by reviewing theoretical predictions of the effect of salinity and temperature on A and B parameters. Next, we evaluate the accuracy of existing empirical methods for calculating A and B parameters in RO/HPRO and A, B, and S parameters in FO, PRO, and OARO processes. The accuracy is evaluated without error in experimental measurements and with the addition of low and high levels of error in the experimental measurements of selected process parameters. This analysis allows us to differentiate between methodological error, namely the effects of simplifying assumptions and empirical approach, and measurement error, on the accuracy of each empirical method for estimating A and B, or A, B, and S.

3.1. Effect of salinity and temperature on membrane water and salt permeability

Transport of water and salt in polymer membranes is primarily dictated by the free volume of water and electrostatic interactions between the dissolved ion and the polymer [10,51,52]. The free volume of water typically decreases as the external salt concentration increases due to osmotic deswelling [10,21,53]. This change in water uptake is also mediated by temperature, where an increase in temperature increases the activity coefficient of water and water uptake by the polymeric material (Fig. 3A).

A decrease in water uptake decreases the water and salt permeability of polymeric membranes. Experimental observations suggest that CTA
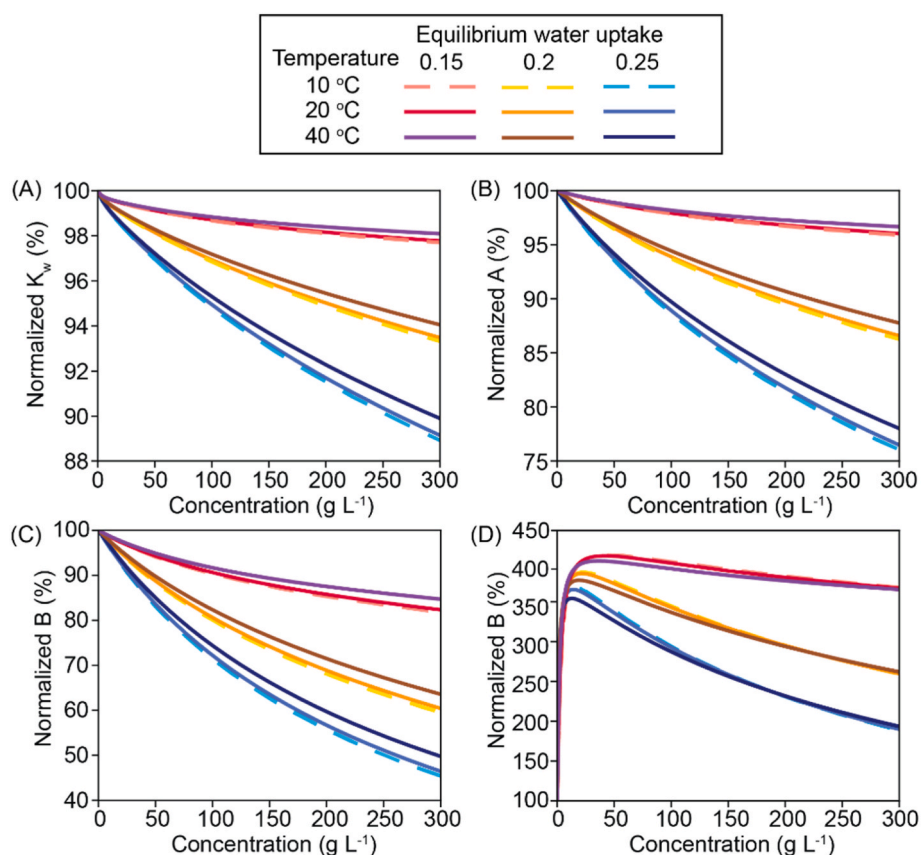
Fig. 3. (A) Normalized water uptake, (B) normalized water permeability coefficient, normalized salt permeability coefficient for (C) uncharged and (D) charged membrane. Membranes with increasing equilibrium water uptake, 0.15, 0.2, and 0.25 in DI water, are simulated across the full salinity range (0–300 g/L) at different temperatures (10 °C, 20 °C, 40 °C).

and TFC-PA polymeric membranes absorb as much as 10%–22% by weight of water in a deionized condition [42,45,54]. The Flory-Rehner theory predicts a decrease in water uptake of as much as 10% as salinity approaches the crystallization point of NaCl (Fig. 3A). In CTA membranes, this 10% decrease in water uptake could reduce water and salt permeability by as much as 25% and 50%, respectively (Fig. 3 B, C).

For charged TFC-PA membranes, the salt permeability is both a function of water uptake and polymer charge. This results in a non-monotonic change of B with increasing salt concentration (Fig. 3D). At low salinities, the fixed charge groups of the membrane limit mobile ion transport through electrostatic repulsion, commonly known as Donnan exclusion [44,45,55]. As salinity increases, ions screen the effective polymer charge and weaken the effect of Donnan exclusion, resulting in an increase in salt permeability. When the effective polymer charge is completely screened, charged polymer membranes behave like uncharged membranes where ion transport becomes governed by ion diffusion through the free water volume of the polymer. High salinity decreases free volume of the polymer, decreasing salt permeability [44].

3.2. Accuracy of empirical methods of membrane parameter estimation in RO

We evaluate the accuracy of the empirical method for estimating A and B parameters in steady-state RO/HPRO processes with fixed over pressure (Fig. 4) and random over pressure (Supplementary Fig. S7). The accuracy of the empirical method depends both on the error introduced by the methodological approach and the error introduced by inaccuracies in experimental measurements. We evaluate the effect of method error and the effect of imprecise measurement by analyzing the errors in estimated membrane parameters solved by the RO method with no

random error and with varying levels of random errors in measured parameters, respectively.

We find that the methodological error in the RO/HPRO empirical method for A and B estimation is low. When no random errors are added to measurement, the method accurately estimated constant and concentration-dependent A and B values across the full salinity range with median and 95th percentile errors of less than 0.1% (Fig. 4 and Supplementary Fig. S7).

While the methodological error is low, the direct estimation method for water permeability and salt permeability in RO/HPRO process is prone to random error in experimental measurements, especially under high salinity conditions (Fig. 4 and Supplementary Fig. S7). When random large errors are introduced to the measured parameters in low salinity case, the median errors in estimated constant A and B parameters increased to 22% and 3%, respectively, and the 95th percentile errors increased to 147% and 7.9%, respectively. In high salinity cases, the median errors in A further increased to 57% and the 95th percentile errors increased to 352%. The errors in B remain nearly constant in both salinity cases.

The effect of large random measurement errors further increased for concentration-dependent A, where median errors for high salinity cases are 63% and 95th percentile errors are 374%. Increasing applied over pressure decreases the impact of measurement errors on the uncertainty of the estimated A parameter (Supplementary Fig. S7). While a more mechanistic explanation will be provided later in Section 3.5, the high uncertainty of the RO method in high salinity conditions far exceeds the theoretically predicted change of A and B across the relevant salinity range (Fig. 3B–D). Thus, the RO method is insufficient for capturing the dependence of A and B on salinity, with the method performing especially poorly in the high salinity range.
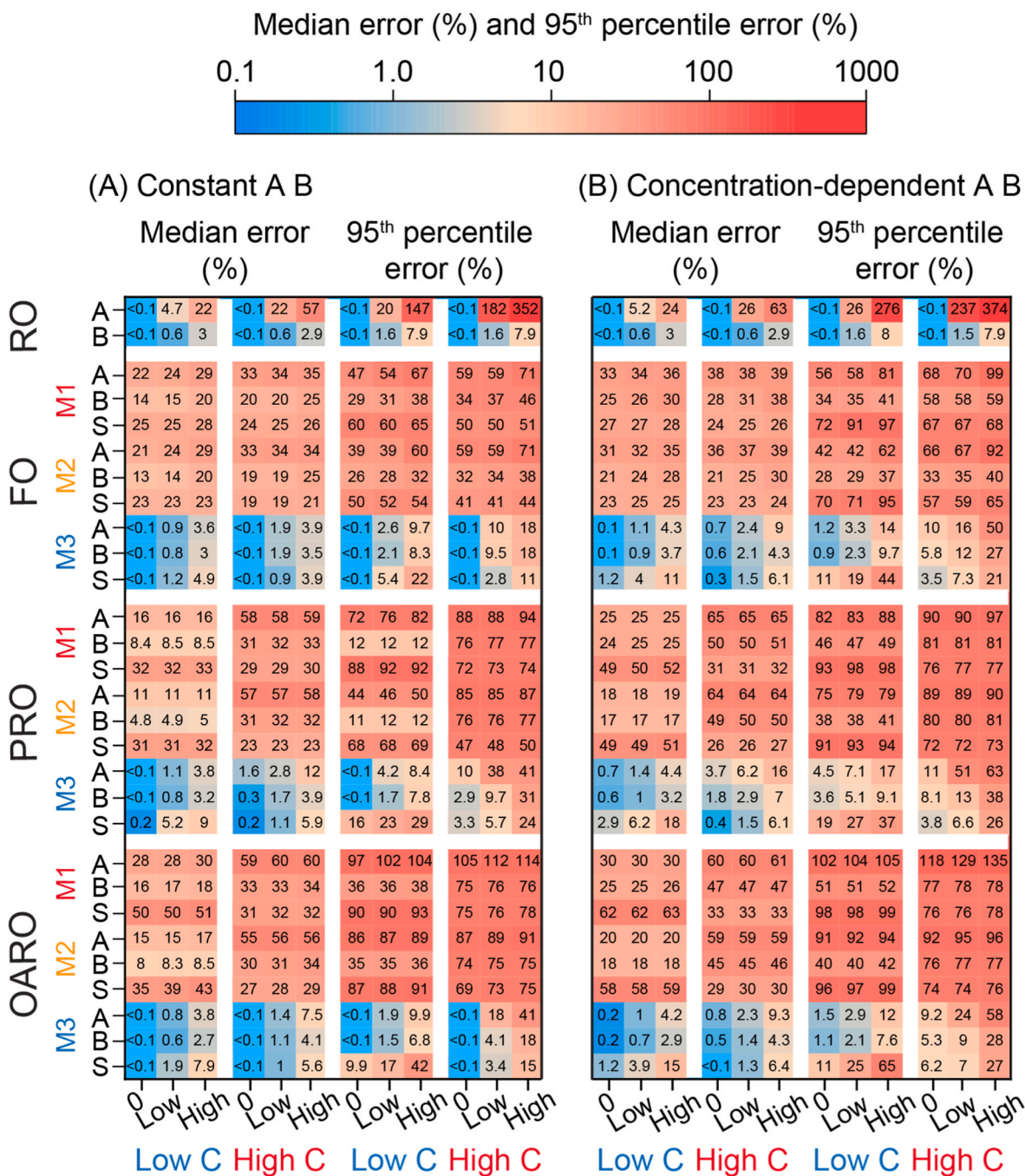
Fig. 4. Heatmap of the median and 95th percentile error predictions on simulated datasets for (A) constant or (B) concentration-dependent membrane transport parameters in RO/HPRO, FO, PRO, and OARO. The X-axis shows the level of error added to all input parameters and concentration range. The low concentration range is 0–50 g/L for all processes, and the high concentration range is 150–200 g/L for HPRO, and 250–300 g/L for the rest. The Y-axis denotes the osmotic membrane process, and the corresponding method for each process, the minor labels show the membrane parameters estimated by the method. The median error represents the middle value of all errors in the estimated membrane parameter in the concentration range, and the 95th percentile error represents the statistical point at which 95% of all errors in estimates are below the reference value in the concentration range. Blue colors indicate a low error in estimated values and red colors indicate a high error in estimated values. The method with high accuracy in predicting membrane parameters will have blue colors (low errors) in its results, whereas a method with poor accuracy will have high errors in its predictions (red colors). (For interpretation of the references to color in this figure legend, the reader is referred to the Web version of this article).

3.3. Accuracy of empirical methods of membrane parameter estimation in FO

The typical operating pressure of RO membranes (<80 bar) precludes the application of direct methods for determining A and B at concentrations exceeding ∼ 85 g/L. To circumvent this constraint, several empirical methods have been developed for estimating A and B

parameters from water and salt flux data collected in FO processes. In addition, these methods consider the transport resistance of the support layer, which is described using a structural parameter, S. As discussed in the introduction and summarized in Fig. 1, these methods make different sets of simplifying assumptions that influence their methodological accuracy (Fig. 4).

The accuracy of the three methods in estimating the physical model

parameters varies substantially across the three methods. Our results suggest that fully accounting for the thermophysical properties of the solution is critical to accurately estimating membrane parameters (Fig. 4). The method with the highest accuracy (M3), derived by Chowdhury et al. and Martin et al., estimated membrane parameters with errors <5% in the absence of random measurement error. This method (M3) included all thermophysical solution properties and ECP layers that form in osmotically assisted processes. In contrast, simpler methods (M1) developed by Tiraferri et al., and (M2) derived by Nagy et al. and Bui et al. assumed constant solution properties and had errors averaging 10–20 times higher than M3.

Critically, these results suggest that current methods are insufficiently precise for resolving changes in A, B, and S with increasing salinity. Free volume theory predicts a maximum expected change in A and B of 25% and 50%, respectively. The most accurate FO method, M3, however, has a median error of 10% and 95th percentile errors as high as 50% when large measurement errors are introduced to the inputs. This magnitude of error makes it impossible to differentiate measurement error from actual changes in membrane parameters. Only for charged membranes at concentrations of less than 50 g/L, where the change in B is 200–300%, is the effect of salinity potentially resolvable using M3.

3.4. Effect of salinity on the accuracy of empirical methods

The error in estimated water permeability increases with increasing concentration in RO/HPRO due to the decrease in effective driving force, whereas the error in estimated salt permeability is minimally affected by the change of effective driving force. In low salinity conditions, the osmotic pressure at the membrane surface is similar to that of the bulk (Fig. 5A), and error in most measured parameters negligibly impacts the estimates of osmotic pressure at the membrane surface. At high feedwater salinities, however, the osmotic pressure at the membrane surface can approach or exceed the applied hydraulic pressure. Even if external concentration polarization is minimal, minor errors in bulk concentration or pressure directly and significantly impact the calculation of effective driving force and water permeability (Supplementary Fig. S8A). In contrast, the error in estimated salt permeability is determined by the estimated salt concentration at the membrane surface ($C_{f,m}$) and the permeate concentration (C_p). The impact of random errors in measurement on estimated $C_{f,m}$ is less significant across the salinity range (Supplementary Fig. S8B). Meanwhile, an increased concentration gradient across the membrane (or high salt flux) with salinity mitigates the effect of random errors in salt concentration on the accuracy of estimating B parameter at high salinity conditions (Fig. 5A).

Errors in estimated water and salt permeability increase with salt concentration in the FO process, whereas errors in estimated structural parameters slightly decrease with the increase in salt concentration (Fig. 4). In FO, increasing draw solution concentration increases the osmotic pressure difference (or effective driving force) across the membrane, leading to increased water permeation and more severe

external and internal concentration polarization. Under these conditions, estimates of salt concentration at the membrane surface are particularly susceptible to bulk concentration measurement errors (Fig. 5B), propagating to poor estimates of the driving force, A, and B parameters. The S parameter, in contrast, is estimated from the concentration gradient across the support layer. The magnitude of this concentration gradient increases with salinity, thus decreasing the impact of random error on its estimate (Fig. 5B). The same conclusion applies to PRO and OARO (Supplementary Fig. S9).

3.5. Effect of individual input error on the accuracy of empirical methods

This analysis is also valuable for identifying experimental errors that adversely impact the estimation accuracy of empirical methods and prioritizing improvements to experimental measurement approaches.

Errors in bulk concentration measurements have the largest impact on estimation accuracy because it directly impacts estimates of the osmotic pressure and the effective driving force. For example, a ±5% error in measured bulk concentration can induce up to 58% and 2.1% errors in A and B parameters, respectively, using the RO method (Fig. 6A and B), and 2.5% and 2.4% errors in A and B parameters, respectively, using the FO method (Fig. 6C and D). Errors in measured bulk concentration come from multiple sources. When the bulk concentration is solely determined from solution preparation, the accuracy of weighing scales of ±0.1% for lab-scale measurements, and the accuracy of volume measurement of ±1% to ±5% for graduated cylinders or beakers can propagate to ±1% to ±5% error in measured concentration [56,57]. Evaporation from the system can also lead to errors over long experimental time periods. In contrast, if the bulk concentration is determined by a conductivity meter, errors in bulk concentration can be reduced to ±1% when the conductivity meter is properly calibrated over the full salinity range. Note that use of an improperly calibrated conductivity probe, the failure to simultaneously monitor temperature, and other instances of improper experimental protocol are not accounted for in our analysis. The imperative of high precision concentration measurements leads to the recommendation that research groups use properly calibrated conductivity meters coupled with temperature monitoring or a temperature control system.

The accuracy of estimated A parameters is also highly dependent on accurate pressure measurements. The standard method estimates the salt concentration on the membrane surface using the film model from measured water flux, salt flux, and bulk concentration (Eqn. (1)). Next, A and B are separately determined by estimating the driving force and concentration difference across the membrane (Eqns. (2) and (3)). As a result, the measured pressure is only used in the calculation of the A parameter. As shown in our analysis, a 5% error in pressure can lead to 19% and 46% errors in A in low and high salinity conditions, respectively (Fig. 6A). The error of pressure measurement directly comes from the resolution of the pressure gauge. Therefore, the use of high precision digital pressure gauges with an accuracy of ±0.05% of span is essential
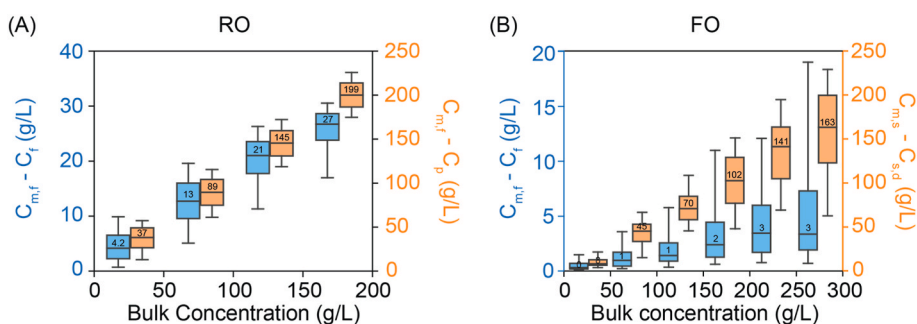

Fig. 5. Range of simulated concentration differences across the membrane and support layer as a function of bulk feed concentration (without added input errors). (A) Concentration difference between membrane surface ($C_{m,f}$) and bulk (C_f), and concentration gradient across the membrane ($C_{m,f}$ − C_p) in RO with a fixed over pressure. (B) Concentration difference between membrane surface ($C_{m,f}$) and bulk (C_f) in FO (blue), and concentration gradient across the support membrane ($C_{m,s}$ − $C_{m,d}$) in FO (orange). The top and bottom of the box represent 25th percentile and 75th percentile values, and the high and low whiskers represent the 5th and 95th percentile differences in concentration. The line and numerical value inside the box represent the median concentration difference. (For interpretation of the references to color in this figure legend, the reader is referred to the Web version of this article).
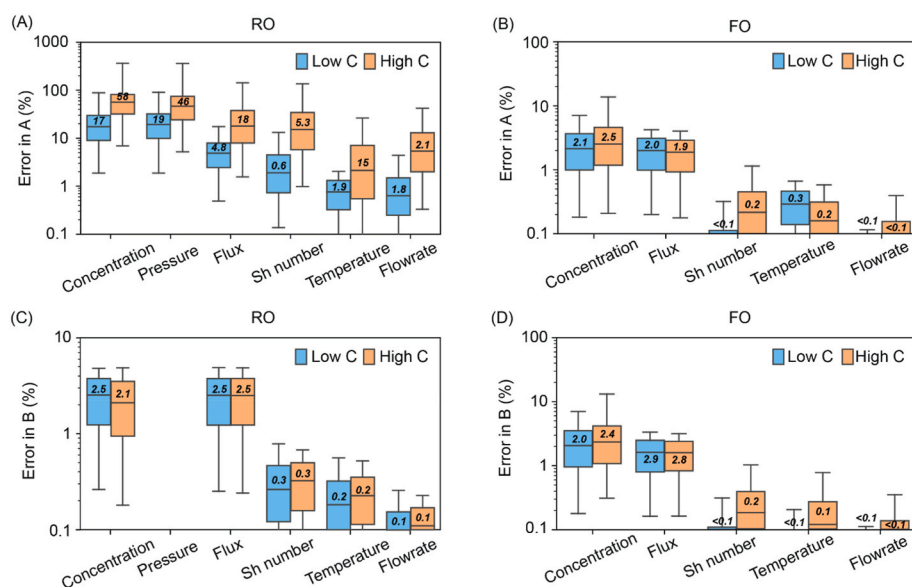
Fig. 6. Effect of 5% random measurement error on empirical method prediction errors of membrane water and salt permeability parameters in RO (with a fixed over pressure) and FO. Analysis assumes constant membrane transport parameters over full salinity range. The line and numerical value inside the box represent the median value of errors in parameters. The top and bottom of the box represent 25th percentile and 75th percentile values, and the high and low whiskers represent the 5th and 95th percentile values. The X-axis shows the error groups added to the input at low concentration range (0–50 g/L, blue box) and high concentration range (150–200 g/L for RO/HPRO, 250–300 g/L for FO, yellow box). Method 3 is used for the error analysis in FO. (For interpretation of the references to color in this figure legend, the reader is referred to the Web version of this article).

for minimizing the errors from pressure readings.

The third highest impact was observed for measurement errors in permeate and salt flux, as they are used to directly estimate the A, B, and S parameters. The potential sources of error in water flux measurement primarily stem from the weight measurement of permeate, which is affected by the accuracy of the weighing scale and actual mass flux from the module. Error in the salt flux is more complicated, as it is estimated from changes in concentration over time (determined using a conductivity meter, the accuracy of which is typically $\pm$1% [58], but needs to be properly calibrated over the full salinity and temperature range of the experiments as described above), water flux, volume measurement of the initial feed solution, and membrane area. For example, a 1% error in each of the parameters results in an average salt flux error of approximately 9%. As shown in our analysis, a 5% error in water or salt flux can result in 18% and 2% errors in estimated water permeability in RO and FO system, respectively, and 2.5% and 2.9% error in estimated salt permeability in RO and FO system, respectively (Fig. 6). Regular calibration of the weighing scale, timer, and conductivity meter, combined with automated data logging system will minimize the effect of random errors in these measurements.

Finally, each of the methods assessed in this work requires ex-situ measurement of Sherwood number in the flow cell. Sherwood number correlations derived for a specific cell often have errors as high as 5%, however application of Sherwood number correlations outside that specific cell can lead to much larger errors in the estimate of mass transport (often on the order of 20–50%) even when using same hydraulic diameter and module length [59–61]. Fortunately, the effect on estimates of A and B are relatively insensitive to error of up-to 5% at low concentrations, though the impact grows as the salinity of the feed increases. Similarly, errors in temperature measurement and flowrate measurement have only moderate effects on the accuracy of most membrane parameter estimates. An exception is the impact of large errors in temperature in RO/HPRO at high salinities on estimated A parameter. This is caused by the uncertainty of effective driving force at high salinities due to the variation in estimated osmotic pressure influenced by temperature errors. Despite the small influence of Sherwood number and temperature on estimated membrane parameters at low salinity, the larger effect at high salinity necessitates high resolution measurement of temperature and crossflow rates using high precision thermometers and flowmeters.

4. Conclusion

We have presented a systematic accuracy analysis of empirical methods in estimating membrane parameters in four osmotic processes including RO/HPRO, FO, PRO, and OARO, with constant and concentration-dependent water and salt permeability across the full salinity range. The results of our analysis suggest that the direct calculation method in RO is the least accurate method for estimating membrane parameters due to this method's high sensitivity to experimental measurement errors. The adoption of a multistage measurement strategy and the inclusion of solution thermophysical properties in empirical models built on FO, PRO and OARO process significantly improve the accuracy of A and B parameter estimates.

We also find that the errors in the estimates of membrane parameters increase with increasing feed salinity. This error stems from the difficulty of accurately estimating the salt concentration at the membrane surface and, thus, the effective driving force. Here, uncertainty from concentration and pressure measurements has the greatest impact on the accuracy of estimated parameters because they directly influence the calculation of driving force. Therefore, we recommend researchers use regularly calibrated high-precision measurement tools and an automated data logging system in order to minimize the effect of random errors in these measurements.

Even the most complete method for estimating A, B, and S parameters at high salinities exhibits impractically large errors. Median errors exceed 10%, while the 5th to 95th percentile error range exceeds 40%. Theoretically predicted A and B change up to 25% and 50% from seawater level to near crystallization point of NaCl for state-of-the-art desalination membranes. If membrane parameters are a function of salinity, these error estimates increase to 20% and 60% for the median and 5th to 95th percentile ranges, respectively. This uncertainty in the true values of A and B makes it exceedingly difficult to resolve the actual effects of feedwater salinity on membrane parameters and assure the performance of membranes in high salinity process applications. Direct or higher accuracy empirical methods must be developed to fully quantify the effect of operating conditions on membrane transport properties.

CRediT authorship contribution statement

Yuanzhe Liang: Conceptualization, Methodology, Investigation, Data curation, Formal analysis, Writing – original draft, review &

editing. **Alexander V. Dudchenko**: Conceptualization, Methodology, Validation, Software, Supervision, Writing – review & editing. **Meagan S. Mauter**: Conceptualization, Investigation, Writing – review & editing, Supervision, Project administration, Funding acquisition.

Declaration of competing interest

The authors declare that they have no known competing financial interests or personal relationships that could have appeared to influence the work reported in this paper.

Data availability

Data will be made available on request.

Appendix A. Supplementary data

Supplementary data to this article can be found online at https://doi.org/10.1016/j.memsci.2022.121246.

References

[1] T.V. Bartholomew, L. Mey, J.T. Arena, N.S. Siefert, M.S. Mauter, Osmotically assisted reverse osmosis for high salinity brine treatment, Desalination 421 (2017) 3–11, https://doi.org/10.1016/j.desal.2017.04.012.

[2] T.V. Bartholomew, N.S. Siefert, M.S. Mauter, Cost optimization of osmotically assisted reverse osmosis, Environ. Sci. Technol. 52 (2018) 11813–11821, https://doi.org/10.1021/acs.est.8b02771.

[3] A. Zhu, A. Rahardianto, P.D. Christofides, Y. Cohen, Reverse osmosis desalination with high permeability membranes-cost optimization and research needs, Desalination Water Treat. 15 (2010) 256–266.

[4] X. Chen, C. Boo, N.Y. Yip, Transport and structural properties of osmotic membranes in high-salinity desalination using cascading osmotically mediated reverse osmosis, Desalination 479 (2020), 114335, https://doi.org/10.1016/j.desal.2020.114335.

[5] Z. Wang, A. Deshmukh, Y. Du, M. Elimelech, Minimal and zero liquid discharge with reverse osmosis using low-salt-rejection membranes, Water Res. 170 (2020), 115317.

[6] D.M. Davenport, A. Deshmukh, J.R. Werber, M. Elimelech, High-pressure reverse osmosis for energy-efficient hypersaline brine desalination: current status, design considerations, and research needs, Environ. Sci. Technol. Lett. 5 (2018) 467–475.

[7] S. Lin, M. Elimelech, Staged reverse osmosis operation: configurations, energy efficiency, and application potential, Desalination 366 (2015) 9–14, n.d.

[8] D.M. Warsinger, E.W. Tow, K.G. Nayar, L.A. Maswadeh, Energy efficiency of batch and semi-batch (CCRO) reverse osmosis desalination, Water Res. 106 (2016) 272–282.

[9] T.Y. Cath, A.E. Childress, M. Elimelech, Forward osmosis: principles, applications, and recent developments, J. Membr. Sci. 281 (2006) 70–87.

[10] G.M. Geise, D.R. Paul, B.D. Freeman, Fundamental water and salt transport properties of polymeric materials, Prog. Polym. Sci. 39 (2014) 1–42, https://doi.org/10.1016/j.progpolymsci.2013.07.001.

[11] O. Coronell, B.J. Mariñas, X. Zhang, D.G. Cahill, Quantification of functional groups and modeling of their ionization behavior in the active layer of FT30 reverse osmosis membrane, Environ. Sci. Technol. 42 (2008) 5260–5266, https://doi.org/10.1021/es8002712.

[12] W. Xie, H. Ju, G.M. Geise, B.D. Freeman, J.I. Mardel, A.J. Hill, J.E. McGrath, Effect of free volume on water and salt transport properties in directly copolymerized disulfonated poly(arylene ether sulfone) random copolymers, Macromolecules 44 (2011) 4428–4438, https://doi.org/10.1021/ma102745s.

[13] T. Fujioka, N. Oshima, R. Suzuki, W.E. Price, L.D. Nghiem, Probing the internal structure of reverse osmosis membranes by positron annihilation spectroscopy: gaining more insight into the transport of water and small solutes, J. Membr. Sci. 486 (2015) 106–118, https://doi.org/10.1016/j.memsci.2015.02.007.

[14] T. Lindfors, F. Sundfors, L. Höfler, róbert E. Gyurcsányi, FTIR ATR study of water uptake and diffusion through ion selective membranes based on plasticized poly (vinyl chloride), Electroanal. An Int. J. Devoted to Fundam. Pract. Asp. Electroanal. 21 (2009) 1914–1922.

[15] C.E. Lamaze, Diffusive and Hydraulic Permeabilities of 9 (1971) 1117–1131.

[16] S. Rosenbaum, H.I. Mahon, O. Cotton, Permeation of water and sodium chloride through cellulose acetate, J. Appl. Polym. Sci. 11 (1967) 2041–2065, https://doi.org/10.1002/app.1967.070111021.

[17] H. Zhang, G.M. Geise, Modeling the water permeability and water/salt selectivity tradeoff in polymer membranes, J. Membr. Sci. 520 (2016) 790–800, https://doi.org/10.1016/j.memsci.2016.08.035.

[18] K. Chang, H. Luo, G.M. Geise, Influence of salt concentration on hydrated polymer relative permittivity and state of water properties, Macromolecules 54 (2021) 637–646, https://doi.org/10.1021/acs.macromol.0c02188.

[19] E.S. Jang, J. Kamcev, K. Kobayashi, N. Yan, R. Sujanani, S.J. Talley, R.B. Moore, D. R. Paul, B.D. Freeman, Effect of water content on sodium chloride sorption in cross-linked cation exchange membranes, Macromolecules 52 (2019) 2569–2579, https://doi.org/10.1021/acs.macromol.8b02550.

[20] V. Freger, Swelling and morphology of the skin layer of polyamide composite membranes: an atomic force microscopy study, Environ. Sci. Technol. 38 (2004) 3168–3175.

[21] M. Stolov, V. Freger, Membrane charge weakly affects ion transport in reverse osmosis, Environ. Sci. Technol. Lett. 7 (2020) 440–445, https://doi.org/10.1021/acs.estlett.0c00291.

[22] Y. Liang, Y. Zhu, C. Liu, K.R. Lee, W.S. Hung, Z. Wang, Y. Li, M. Elimelech, J. Jin, S. Lin, Polyamide nanofiltration membrane with highly uniform sub-nanometre pores for sub-1 Å precision separation, Nat. Commun. 11 (2020) 1–9, https://doi.org/10.1038/s41467-020-15771-2.

[23] W. Cheng, C. Liu, T. Tong, R. Epsztein, M. Sun, R. Verduzco, J. Ma, M. Elimelech, Selective removal of divalent cations by polyelectrolyte multilayer nanofiltration membrane: role of polyelectrolyte charge, ion size, and ionic strength, J. Membr. Sci. 559 (2018) 98–106, https://doi.org/10.1016/j.memsci.2018.04.052.

[24] L. Wang, T. Cao, J.E. Dykstra, S. Porada, P.M. Biesheuvel, M. Elimelech, Salt and water transport in reverse osmosis membranes: beyond the solution-diffusion model, Environ. Sci. Technol. 55 (24) (2021) 16665–16675, https://doi.org/10.1021/acs.est.1c05649.

[25] E.S. Jang, J. Kamcev, K. Kobayashi, N. Yan, R. Sujanani, T.J. Dilenschneider, H. B. Park, D.R. Paul, B.D. Freeman, Influence of water content on alkali metal chloride transport in cross-linked Poly(ethylene glycol) diacrylate.2. Ion diffusion, Polymer 192 (2020), 122316, https://doi.org/10.1016/j.polymer.2020.122316.

[26] G.M. Geise, C.M. Doherty, A.J. Hill, B.D. Freeman, D.R. Paul, Free volume characterization of sulfonated styrenic pentablock copolymers using positron annihilation lifetime spectroscopy, J. Membr. Sci. 453 (2014) 425–434.

[27] H.Y. Ng, W. Tang, W.S. Wong, Performance of forward (direct) osmosis process: membrane structure and transport phenomenon, Environ. Sci. Technol. 40 (2006) 2408–2413.

[28] M.F.A. Goosen, S.S. Sablani, S.S. Al-Maskari, R.H. Al-Belushi, M. Wilf, Effect of feed temperature on permeate flux and mass transfer coefficient in spiral-wound reverse osmosis systems, Desalination 144 (2002) 367–372.

[29] Z.F. Wang, B. Wang, X.M. Ding, M. Zhang, L.M. Liu, N. Qi, J.L. Hu, Effect of temperature and structure on the free volume and water vapor permeability in hydrophilic polyurethanes, J. Membr. Sci. 241 (2004) 355–361.

[30] M.A. Ebrahim, S. Karan, A.G. Livingston, On the influence of salt concentration on the transport properties of reverse osmosis membranes in high pressure and high recovery desalination, J. Membr. Sci. 594 (2020), 117339.

[31] R.W. Baker, Membrane Technology and Applications, John Wiley & Sons, 2012, https://doi.org/10.1002/9781118359686.

[32] R.K. McGovern, D. McConnon, J.H. Lienhard V, The Effect of Very High Hydraulic Pressure on the Permeability and Salt Rejection of Reverse Osmosis Membranes, 2015.

[33] A. Tiraferri, N.Y. Yip, A.P. Straub, S. Romero-Vargas Castrillon, M. Elimelech, A method for the simultaneous determination of transport and structural parameters of forward osmosis membranes, J. Membr. Sci. 444 (2013) 523–538, https://doi.org/10.1016/j.memsci.2013.05.023.

[34] E. Nagy, A general, resistance-in-series, salt-and water flux models for forward osmosis and pressure-retarded osmosis for energy generation, J. Membr. Sci. 460 (2014) 71–81.

[35] N.-N. Bui, J.T. Arena, J.R. McCutcheon, Proper accounting of mass transfer resistances in forward osmosis: improving the accuracy of model predictions of structural parameter, J. Membr. Sci. 492 (2015) 289–302.

[36] M.R. Chowdhury, J.R. McCutcheon, Elucidating the impact of temperature gradients across membranes during forward osmosis: coupling heat and mass transfer models for better prediction of real osmotic systems, J. Membr. Sci. 553 (2018) 189–199.

[37] J.T. Martin, G. Kolliopoulos, V.G. Papangelakis, An improved model for membrane characterization in forward osmosis, J. Membr. Sci. 598 (2020), 117668, https://doi.org/10.1016/j.memsci.2019.117668.

[38] A.V. Dudchenko, M.S. Mauter, Neural networks for estimating physical parameters in membrane distillation, J. Membr. Sci. 610 (2020), 118285, https://doi.org/10.1016/j.memsci.2020.118285.

[39] P.J. Flory, Principles of polymer chemistry, Choice Rev. Online. 33 (1995) 33–2140, https://doi.org/10.5860/choice.33-2140. -33–2140.

[40] J.C. Bray, E.W. Merrill, Poly (vinyl alcohol) hydrogels. Formation by electron beam irradiation, J. Appl. Polym. Sci. 17 (1973) 3779–3794.

[41] H. Lin, T. Kai, B.D. Freeman, S. Kalakkunnath, D.S. Kalika, The effect of cross-linking on gas permeability in cross-linked poly(ethylene glycol diacrylate), Macromolecules 38 (2005) 8381–8393, https://doi.org/10.1021/ma0510136.

[42] E.S. Jang, J. Kamcev, K. Kobayashi, N. Yan, R. Sujanani, T.J. Dilenschneider, H. B. Park, D.R. Paul, B.D. Freeman, Influence of water content on alkali metal chloride transport in cross-linked Poly(ethylene glycol) Diacrylate.1. Ion sorption, Polymer 178 (2019), 121554, https://doi.org/10.1016/j.polymer.2019.121554.

[43] H.B. Park, A.C. Sagle, J.E. McGrath, B.D. Freeman, Water permeability and water/salt selectivity tradeoff in polymers for desalination, AIChE Annu. Meet. Conf. Proc. 369 (2008) 130–138.

[44] G.M. Geise, L.P. Falcon, B.D. Freeman, D.R. Paul, Sodium chloride sorption in sulfonated polymers for membrane applications, J. Membr. Sci. 423–424 (2012) 195–208, https://doi.org/10.1016/j.memsci.2012.08.014.

[45] F.G. Helfferich, Ion Exchange, Courier Corporation, 1995.

[46] J.G. Wijmans, R.W. Baker, The solution-diffusion model : Rev. 107 (1995) 1–21.

[47] D.R. Paul, Reformulation of the solution-diffusion theory of reverse osmosis, J. Membr. Sci. 241 (2004) 371–386, https://doi.org/10.1016/j.memsci.2004.05.026.

[48] K.G. Nayar, M.H. Sharqawy, L.D. Banchik, J.H. Lienhard, Thermophysical properties of seawater: a review and new correlations that include pressure dependence, Desalination 390 (2016) 1–24, https://doi.org/10.1016/j.desal.2016.02.024.

[49] N.Y. Yip, A. Tiraferri, W.A. Phillip, J.D. Schiffman, L.A. Hoover, Y.C. Kim, M. Elimelech, Thin-film composite pressure retarded osmosis membranes for sustainable power generation from salinity gradients, Environ. Sci. Technol. 45 (2011) 4360–4369.

[50] P. Virtanen, R. Gommers, T.E. Oliphant, M. Haberland, T. Reddy, D. Cournapeau, E. Burovski, P. Peterson, W. Weckesser, J. Bright, SciPy 1.0: fundamental algorithms for scientific computing in Python, Nat. Methods 17 (2020) 261–272.

[51] Y. Liang, S. Lin, Mechanism of permselectivity enhancement in polyelectrolyte-dense nanofiltration membranes via surfactant-assembly intercalation, Environ. Sci. Technol. 55 (1) (2020) 738–748, https://doi.org/10.1021/acs.est.0c06866.

[52] Y. Liang, S. Lin, Intercalation of zwitterionic surfactants dramatically enhances the performance of low-pressure nanofiltration membrane, J. Membr. Sci. 596 (2020), 117726, https://doi.org/10.1016/j.memsci.2019.117726.

[53] J.R. McCutcheon, R.L. McGinnis, M. Elimelech, Desalination by ammonia-carbon dioxide forward osmosis: influence of draw and feed solution concentrations on process performance, J. Membr. Sci. 278 (2006) 114–123.

[54] A.R. Khare, N.A. Peppas, Swelling/deswelling of anionic copolymer gels, Biomaterials 16 (1995) 559–567.

[55] G.M. Geise, H.S. Lee, D.J. Miller, B.D. Freeman, J.E. McGrath, D.R. Paul, Water purification by membranes: the role of polymer science, J. Polym. Sci., Part B: Polym. Phys. 48 (2010) 1685–1718.

[[56]] P. Patnaik, Dean's Analytical Chemistry Handbook, McGraw-Hill Education, 2004.

[57] J. Wagner, Membrane filtration handbook, Pract. Tips Hints. Osmonics. (2001).

[58] T.J. Day, On the precision of salt dilution gauging, J. Hydrol. 31 (1976) 293–306.

[59] M.E. Leitch, G.V. Lowry, M.S. Mauter, Characterizing convective heat transfer coefficients in membrane distillation cassettes, J. Membr. Sci. 538 (2017) 108–121.

[60] A.V. Dudchenko, M. Hardikar, R. Xin, S. Joshi, R. Wang, N. Sharma, M.S. Mauter, Impact of module design on heat transfer in membrane distillation, J. Membr. Sci. 601 (2020), 117898.

[61] A.V. Dudchenko, T.V. Bartholomew, M.S. Mauter, High-impact innovations for high-salinity membrane desalination, Proc. Natl. Acad. Sci. USA 118 (2021).